

XR-VLM: Cross-Relationship Modeling with Multi-part Prompts and Visual Features for Fine-Grained Recognition

Chuanming Wang Hengming Mao Huanhuan Zhang Huiyuan Fu Huadong Ma

The State Key Laboratory of Networking and Switching Technology
Beijing University of Posts and Telecommunications

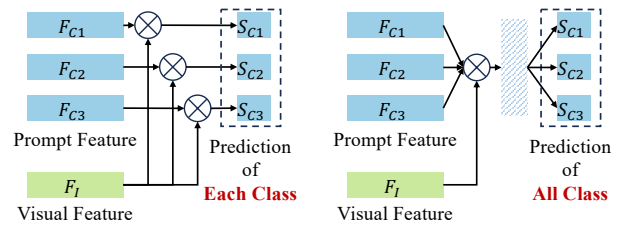
{wcm, maohengming, zhanghuanhuan, fhy, mhd}@bupt.edu.cn

Abstract

Vision-Language Models (VLMs) have demonstrated impressive performance on various visual tasks, yet they still require adaptation on downstream tasks to achieve optimal performance. Recently, various adaptation technologies have been proposed, but we observe they often underperform in fine-grained visual recognition, which requires models to capture subtle yet discriminative features to distinguish similar sub-categories. Current adaptation methods typically rely on an alignment-based prediction framework, i.e. the visual feature is compared with each class prompt for similarity calculation as the final prediction, which lacks class interaction during the forward pass. Besides, learning single uni-modal feature further restricts the model’s expressive capacity. Therefore, we propose a novel mechanism, XR-VLM, to discover subtle differences by modeling cross-relationships, which specifically excels in scenarios involving multiple features. Our method introduces a unified multi-part visual feature extraction module designed to seamlessly integrate with the diverse backbones inherent in VLMs. Additionally, we develop a multi-part prompt learning module to capture multi-perspective descriptions of sub-categories. To further enhance discriminative capability, we propose a cross relationship modeling pattern that combines visual feature with all class prompt features, enabling a deeper exploration of the relationships between these two modalities. Extensive experiments have been conducted on various fine-grained datasets, and the results demonstrate that our method achieves significant improvements compared to current state-of-the-art approaches. Code will be released.

1. Introduction

Vision-Language Models (VLMs) [13, 22, 29, 33, 34] have achieved significant success by using contrastive learning



(a) Illustration of Aligning Pattern. (b) Illustration of Crossing Pattern.

Figure 1. Comparison between (a) previous prediction pattern, generated by aligning a single visual feature with each class prompt feature individually (referred to as the *aligning pattern*), and (b) our prediction pattern, generated by modeling cross relationship between a single visual feature and all class prompt features collectively (referred to as the *crossing pattern*)

to project images and texts into a shared feature space during pre-training, which has encouraged researchers to adapt these models for various downstream tasks. However, due to the need of processing both vision and language data, VLMs typically contain a huge number of parameters, making them substantially more resource-intensive than traditional backbones [7, 25]. As a result, fine-tuning all parameters in these models is not practical due to its massive requirements of considerable data and computational resources. To address these challenges, a growing number of studies [9, 31, 39] have focused on optimizing specific modules within VLMs rather than fine-tuning the entire model. In the literature, prompt learning and adapter learning have emerged as promising paradigms, recognized for their flexibility and efficiency in enhancing VLM performance across various downstream tasks.

Prompt learning [4, 39, 41] focuses on the optimization of language input by designing task-specific textual prompts that guide the model to generate more relevant and context-aware features. On the other hand, adapter learning methods insert lightweight, task-specific modules into the pre-trained model, enabling improve the discriminativeness of

outputs from both the vision and language branches. Despite differences in the parameters being fine-tuned, these methods still rely on an alignment-based pattern for prediction. As illustrated in Fig. 1a, the visual feature is compared with each class prompt feature, and the resulting similarity is used as the logit for the corresponding class. However, we find that such a prediction pattern is not well-suited for fine-grained visual recognition (FGVR) [35], a task that requires distinguishing highly similar sub-categories within a broader class (e.g., differentiating bird species or car models). The similarity among these sub-categories is significantly higher compared to coarse-grained classes (a simple evaluation experiment demonstrating this is provided in the supplementary material), often leading to confusion in predictions. Furthermore, previous methods typically output a single feature for both vision and language branches, which restricts the model’s expressive capacity.

To address this issue, we argue that modeling relationships is crucial for FGVR and the final prediction should be taken by considering all class information. Therefore, we propose a Cross-Relationship modeling method (XR-VLM), that captures interactions across prompts and visual features. As shown in Fig. 1b, the key distinction between our and previous methods is that we aggregate the similarities between a visual feature and all class prompts into a relationship representation, which is then used for predicting the logits of all classes. It can be seen as shifting from a 1-to-1 alignment to a 1-to-many comparison scheme. As a result, the final prediction P_i of class i incorporates information from all other classes, enabling richer contextual reasoning. Additionally, we introduce a multi-part prompt and visual feature learning strategy to enhance the expressiveness of learned features, further supporting the modeling of cross relationships.

To evaluate our method, we conduct extensive experiments on various fine-grained benchmark datasets, comparing it with state-of-the-art (SoTA) VLM adaptation methods. Experimental results demonstrate that our approach achieves significant improvements over SoTA methods and attains the best performance on nearly all datasets. Extensive quantitative and visual analyses further confirm that modeling class relationships leads to better performance compared to traditional alignment-based patterns, and learning multiple prompts and visual features per class further enhances VLMs’ effectiveness on FGVR.

The contributions can be summarized as follows:

- We propose a multi-part prompt and visual feature learning framework for VLMs, designed to fully harness the complementary strengths of both vision and language information, enabling more precise capture of subtle differences across similar classes.
- We introduce a cross-relationship modeling scheme to replace the traditional alignment-based prediction pattern.

It enables richer interactions among classes and allow the model to incorporate contextual information from other classes during prediction.

- Extensive experiments on fine-grained benchmarks demonstrate consistent improvements over state-of-the-art methods, validating the effectiveness of our method.

2. Related Works

2.1. Vision-Language Models

Foundational Vision-Language Models (VLMs) leverage both vision and language modalities to learn rich multi-modal representations. These models utilize a self-supervised paradigm, trained on large-scale image-text pairs from the web, enabling impressive performance across various downstream applications. However, efficiently adapting these pre-trained models to specific tasks remains a significant challenge. Conventional fine-tuning methods, which involve optimizing all parameters of the pre-trained network, are impractical due to the large number of parameters and the high computational resources. As a solution, prompt learning [14, 15, 18, 38, 39] has been proposed, which aims at learning suitable additional context on the input text data. Existing work has primarily focused on how to learn prompts for downstream tasks. For example, PromptSRC [15] uses original features to regularize the prompt learning process; PromptKD [18] interpolates a distillation framework to transfer knowledge from a large teacher network to a small student network by prompts. There are some works learn both text and visual prompts, e.g. MaPLE [14] learns prompts for both the image and text branches simultaneously. Adapter learning is another paradigm for VLM adaptation, which focus on integrate additional modules to the pre-trained model and only fine-tuning such modules to boost the discriminativeness of output features. For example, CLIP-adapter [6] adopts an additional bottleneck layer to learn residual feature blending with the original outputs, MMA [31] projects vision and language features into a share space for fine-tuning, Tip-Adapter-F [36] adds a nonlinear, quadratic-complexity module and blends the class scores with the original textual features by evaluating the pairwise similarities between the features of the support sets. However, these methods typically use a single prompt per class and rely on conventional 1-to-1 alignment for prediction, which is not ideal for FGVR. In contrast, we propose a framework that utilizes cross-relationship representations to improve the prediction of similar classes in FGVR task.

2.2. Fine-grained Visual Recognition

FGVR aims to distinguish different sub-categories from one general super-class, which is crucial for many real-world applications. As a result, significant progress has been

made in this field over the past few decades. The related literature can be broadly divided into two groups: part-based [5, 23, 35] and part-free methods [19, 32, 37]. Part-based methods are driven by the need to differentiate similar sub-categories by capturing subtle differences in discriminative parts. They focus on learning to locate and emphasize various part regions using detection [24] or attention [10] sub-networks, followed by feature extraction for classification. In contrast, part-free methods enhance the backbone model’s recognition ability by re-weighting features [27], high-order pooling techniques [19], or employing augmented samples [37] during training. Both types of methods follow the traditional classification paradigm, where an input image is processed by a visual backbone to extract deep features, which are then mapped to a pre-defined class space using a Multilayer Perceptron (MLP). However, VLMs are trained under fundamentally different settings, making direct comparisons with these methods challenging. Therefore, to ensure a fair comparison, we exclude these methods from our experiments.

2.3. Multiple Feature Learning

Multiple feature learning has been widely used in computer vision fields. For example, MCTrans [30] embeds multiple class tokens into the Vision Transformer (ViT) backbone, and it obtains semantic segmentation results of input images by calculating the similarity between different class tokens and patch tokens. AP-Net [1] adopts an attention pyramid module to obtain multiple features progressively, and it combines them to calculate similarities between query and gallery images. Specially, learning multiple features is an important mechanism that can boost models’ performance on various FGVR tasks. For example, WS-DAN [11], CAL [23], and MEPR [26] design different attention module to produce multiple part features for classification. These methods focus on how to ensure the diversity of extracted features by different loss functions or attention generation operations. While our method also involves learning multi-part features, it uniquely emphasizes the learning and utilization of multiple textual prompts. A related work is PLOT [2], which also employs multiple prompts and aligns them with local features using an optimal transport algorithm. In contrast, we introduce a multi-part feature extraction module for visual data, enriching feature semantics for prediction. More importantly, PLOT still adheres to the aligning pattern for prediction, which fundamentally differs from our method.

3. Method

In this section, we begin by introducing the fundamental processes of VLMs and prompt learning. Next, we briefly provide an overview of our proposed XR-VLM, demonstrating how multi-part prompts and visual features are uti-

lized into the framework. Finally, we detail the implementation of each module in our method.

3.1. Preliminary

Vision-Language Models. Following previous works [2, 12, 39], we adopt CLIP as our foundation model, which comprises two branches: an image encoder and a text encoder. Denoting the image encoder as f^I and the text encoder as f^T , contrastive learning is applied between the input image x and their corresponding textual descriptions $D^T = \{t_1, t_2, \dots, t_N\}$ in a prediction form.

$$\text{logits}(y = i|x) = \mu(f^I(x)) \cdot \mu(f^T(t_i))^\top \quad (1)$$

where μ is a normalization function for a vector defined as $\mu(x) = \frac{x}{\|x\|_2}$. Then, the output logit is used to calculate the cross-entropy loss to optimize both encoders. This process is conducted during the pre-training phase, and subsequent works have adopted a same operation in adapting to downstream tasks. Although the softmax function is used to map logits into a probability distribution for loss calculation—where class logits influence each other—this interaction occurs too late in the process. Thus, the model’s ability to capture nuanced relationships between classes during the forward pass remains limited, which is particularly critical for FGVR.

Prompt Learning. In the original CLIP model, the textual descriptions are collected from the web and fixed during pre-training. Rather than relying on manually crafted prompts, recent work has proposed adaptively learning soft textual prompts for downstream tasks. Specifically, some learnable vectors are concatenated with the class name to create a contextualized representation. In this approach, the prompt for a class is represented as $t_i = [V_1][V_2] \cdots [V_M][C_k]$, where each vector $[V_j]$ is a learnable parameter and it has the same dimension as the word embeddings of class name $[C_k]$.

3.2. Framework

The overall framework of XR-VLM is illustrated in Fig. 2. Multi-part prompts are fed into the text encoder to generate multi-part prompt features, while the input image is processed by the image encoder and transformed into multi-part visual features through an unified attention module. Subsequently, cross-relationship modeling is applied to these features to produce a cross-relationship representation, which is used for final prediction by a MLP module.

3.3. Multi-part Prompt Learning

Unlike previous prompt learning methods that typically use a single prompt per class, we pre-define multiple prompts for each class, each representing a different part description.

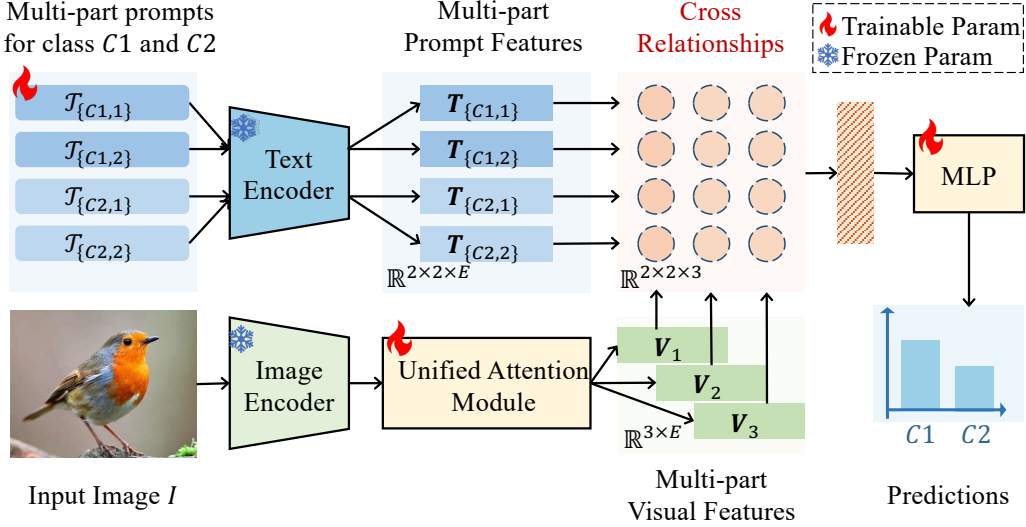


Figure 2. Overall framework of our proposed XR-VLM: For the text branch, multi-part learnable prompts of classes are fed into the Text Encoder, generating multi-part prompt features. For the image branch, the input image is processed through the Image Encoder and an Unified Attention module to generate multi-part visual features. These prompt and visual features are sent to generate the cross-relationship representations, which is finally sent to a MLP module to generate the predictions. (best view in color)

The set of multi-part prompts for a given class, which are fed into the text encoder, is defined as:

$$\mathcal{T}_k = \bigcup_i^S \{ [V_1^i][V_2^i] \cdots [V_M^i][C_k] \}, \quad (2)$$

where $[V_m^s] \in \mathbb{R}^E$ ($s \in 1, \dots, S$, $m \in 1, \dots, M$) represents a vector with dimension E , matching the size of word embeddings, M denotes the number of context of each part prompts, S is the number of part prompts for each class, and $[C_k]$ is the word embedding of the k -th class name. The operation \bigcup refers to the union of sets. As described in [39], in \mathcal{T}_k , all $[V_j^i]$ are learnable, meaning they can be optimized via backward gradients. These pre-defined multi-part prompts are fed into the text encoder to produce the text features $\mathbf{T} \in \mathbb{R}^{W \times S \times E}$, where W is the number of classes and E is the feature dimension. Note that we do not share prompts across classes, as we find that doing so negatively impacts performance as the results reported in [39]. Instead, each class has its unique set of multi-part prompts.

3.4. Multi-part Visual Feature Learning

Denoted the deep features learned by the visual encoder (e.g. ResNet [7] or ViT-B/16 [3]) as $\mathbf{X} \in \mathbb{R}^{N \times E}$ (details is described in supplementary material), where N and E mean the number and channel dimension of features, respectively, we first adopt an effective *Unified Attention* (UnA) module to generate multi-part visual features according to the attentions generated by:

$$\mathbf{A} = \phi(\mathbf{X}; \mathbf{W}_\phi) \in \mathbb{R}^{N \times S}. \quad (3)$$

In detail, ϕ is made up of a BatchNorm layer, a Linear layer, and a ReLU layer. The output dimension of the Linear layer is set to S , so there will be S visual part features as a result, which is same with the number of prompts for each class, and each attention will respond to a particular pattern of object parts. Inspired by [26], to make the learned attentions diverse, we adopt a redundant strategy for \mathbf{A} . First, we change the output dimension of ϕ to $S + 1$, and then we apply a softmax operation along the second dimension of \mathbf{A} :

$$\bar{\mathbf{A}}_{i,s} = \frac{\exp(\mathbf{A}_{i,s})}{\sum_{s=1}^{S+1} \exp(\mathbf{A}_{i,s})}. \quad (4)$$

Next, we select the first S attention maps from $\bar{\mathbf{A}}$ and combine it with \mathbf{X} to produce multiple part features:

$$\mathbf{V} = \bar{\mathbf{A}}^\top \otimes \psi(\mathbf{X}; \mathbf{W}_\psi) \in \mathbb{R}^{S \times E}. \quad (5)$$

ψ is a linear layer with parameter \mathbf{W}_ψ , which projects the visual feature to the relationship learning space, and \otimes denotes the matrix multiplication. Through this way, the first S attention will focus on different parts of object while the remained attention will concentrate on the background, and discriminative information will be brought into part features. Finally, we apply a ℓ_2 normalization on part features:

$$\mathbf{V}_{i,j} = \frac{\mathbf{V}_{i,j}}{\sum_{s=1}^S \sum_{e=1}^E |\mathbf{V}_{s,e}|^2} * \tau, \quad (6)$$

where τ is a scale factor, and we set it to 64.0 as default.

3.5. Cross Relationship Modeling

By incorporating the above modules, we obtain multiple textual features from multi-part prompts and multiple visual features from a single input image. The key challenge

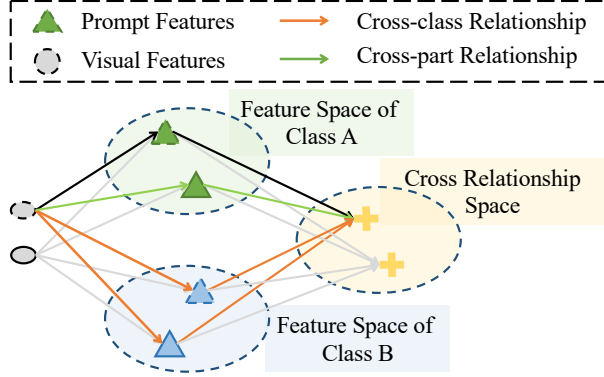


Figure 3. Illustration of cross relationships. Different shape borders represent different parts. (best view in color)

lies in effectively utilizing the rich information contained in these features to achieve precise classification. An alternative strategy is to compute the distance between corresponding visual and textual features for each part type and aggregate the results as the final prediction (called as Part-wise Cosine Similarity, PwCS), which can be defined as:

$$\hat{\mathbf{y}}^{\text{PwCS}} = \frac{1}{S} \sum_{s=1}^S \mu(\mathbf{V}_s) \otimes \mu(\mathbf{T}_{\cdot,s}) \in \mathbb{R}^W. \quad (7)$$

However, as discussed in the introduction, this 1-to-1 distance calculation scheme has limited the expression of VLMs for FGVR. Therefore, we propose a termed *1-to-many relationship learning* scheme, *i.e.* modeling cross relationship to explore the differences and similarities between the learned representations of multi-part prompts and visuals for prediction, termed as *Cross Relationship Modeling* (CRM) module in our method. We re-arrange the shape of \mathbf{T} to $E \times S \times W$ via a transpose operation. The cross-relationship matrix \mathbf{R} of each visual data is calculated as:

$$\mathbf{R} = \epsilon(\mathbf{V} \otimes \mathbf{T}) \in \mathbb{R}^{SSW}, \quad (8)$$

where ϵ is a flatten operation. Then, we treat it as a representation of visual data for classification by a classifier ϑ :

$$\hat{\mathbf{y}}^{\text{CRM}} = \vartheta(\mathbf{R}; W_\vartheta) \in \mathbb{R}^W, \quad (9)$$

where ϑ is the classifier that consists of an MLP (FC-BN-ReLU-FC). This classifier ϑ can be seen as one type of parameterized metric function, which measure the similarity between visual data and multi-part prompts of all class in an implicit manner.

In Fig. 3, we give an illustration of cross relationship. Taking the upper visual feature as an example, given the feature spaces of class *A* and class *B*, our method not only considers part-wise similarities (black lines) but also incorporates cross-part (green lines) and cross-class (orange

lines) relationships. These relationships are projected into a unified space, where optimizing the distances within this space simultaneously influences all relationships. By comprehensively considering both similarities and differences across all classes, the model can capture subtle yet discriminative features, significantly enhancing its ability to distinguish fine-grained sub-categories.

4. Experiments

4.1. Experimental Settings

Datasets. Experiments are conducted on five widely used fine-grained visual recognition benchmark datasets: CUB-200-2011 [28], Stanford-Cars [17], Stanford-Dogs [16], FGVC-Aircraft [20], and NABirds [8]. The training and test sets are constructed following the settings established in prior works [18, 31, 38, 39].

Optimize Configures. CLIP [22] is adopted as the foundational VLM for experiments and we keep its image encoder and text encoder fixed during training. Only parameters in multi-part prompts, UnA module and MLP are used for optimization. We use SGD as the optimizer and set its weight-decay to $1e-4$. We train the models with 100 epochs for all experiments. The learning rate is set to $2e-3$ and is adjusted by cosine learning rate schedule. As the defaults, M is set to 16 and S is set to 4. Following previous methods, for each class, 16 samples are randomly selected from the training set and the model is evaluated on all testing samples.

4.2. Comparison with SoTAs

We compare the performance of XR-VLM against a range of state-of-the-art methods: ZS-CLIP [22], CLIP-Adapter [6], LP-CLIP [22], CoOp [39], PLOT [2], MaPLE [14], MMA [31], LP++ [12], ProGrad [40], PromptSRC [15], and Tip-Adapter-F [36]. Notably, some methods, such as MaPLE and MMA, are specifically designed for a single type of encoder (e.g., Vision Transformers), and thus their results are only reported for that specific architecture.

The experimental results are presented in Table 1, and the methods are sorted by *AVG.* column. From the results, it is evident that our proposed method achieves significant improvements over all compared baselines across most benchmark datasets. Specifically, XR-VLM outperforms existing methods on both RN50 and ViT-B/16 encoders, achieving the highest accuracy on CUB-200-2011, Stanford-Cars, Stanford-Dogs, FGVC-Aircraft, and NABirds datasets. For instance, on the RN50 encoder, XR-VLM achieves an average accuracy of 69.5%, surpassing the second-best method (Tip-Adapter-F) by a notable margin. Similarly, on the ViT-B/16 encoder, XR-VLM attains an average accuracy of 74.9%, further solidifying its superiority.

Prompt learning methods, such as CoOp, ProGrad, and

Visual Encoder	Methods	CUB-200-2011	Stanford-Cars	Stanford-Dogs	FGVC-Aircraft	NABirds	AVG.
RN50	ZS-CLIP [22] _{ICML'21}	45.3	55.7	52.3	17.2	36.5	41.4
	CLIP-Adapter [6] _{IJCV'22}	55.8	63.5	58.5	21.9	45.5	49.0
	LP-CLIP [22] _{ICML'21}	64.1	70.0	52.9	36.0	50.1	54.6
	ProGrad [40] _{ICCV'23}	64.2	73.3	65.6	30.3	46.2	55.9
	PLOT [2] _{ICLR'23}	67.3	73.0	65.2	30.4	45.6	56.3
	CoOp [39] _{IJCV'22}	67.0	73.0	63.9	31.4	47.8	56.6
	LP++ [12] _{CVPR'24}	67.3	72.7	62.1	31.6	51.4	57.0
	Tip-Adapter-F [36] _{ECCV'22}	69.9	74.3	63.6	35.2	56.2	59.8
	XR-VLM(Ours)	75.7	81.8	68.8	53.5	67.7	69.5
ViT-B/16	ZS-CLIP [22] _{ICML'21}	55.0	65.3	61.2	24.7	44.2	50.1
	MaPLE [14] _{CVPR'23}	68.2	73.9	73.9	36.9	55.9	61.8
	ProGrad [40] _{ICCV'23}	73.7	81.9	74.1	41.1	59.9	66.1
	LP++ [12] _{CVPR'24}	74.9	80.9	72.7	41.7	60.7	66.2
	LP-CLIP [22] _{ICML'21}	76.9	80.6	65.5	45.6	64.9	66.7
	CoOp [39] _{IJCV'22}	76.7	82.2	74.2	43.4	61.4	67.6
	PromptSRC [15] _{ICCV'23}	75.3	80.5	76.9	44.2	61.6	68.1
	MMA [31] _{CVPR'24}	76.3	80.8	76.9	43.4	64.1	68.3
	Tip-Adapter-F [36] _{ECCV'22}	79.1	83.7	73.5	44.6	68.2	69.8
	PLOT [2] _{ICLR'23}	77.6	84.4	77.0	46.7	64.3	70.0
XR-VLM(Ours)	81.1	86.5	75.2	57.4	74.1	74.9	

Table 1. Comparison results for fine-grained visual recognition. The highest accuracy is marked as bold.

MaPLE, improve over zero-shot CLIP but often struggle to capture fine-grained details due to their reliance on single-prompt and aligning pattern. In contrast, XR-VLM’s multi-part prompt and cross-relationship modeling address this limitation by enabling richer feature interactions. Adapter-based methods, such as Tip-Adapter-F, show competitive performance but are constrained by their alignment-based prediction patterns, which limit their ability to model complex relationships between classes. XR-VLM’s cross-relationship modeling provides a more comprehensive approach to feature interaction, resulting in superior performance. Linear probing methods, such as LP-CLIP and LP++, while simple, lack the flexibility to model fine-grained relationships, leading to lower accuracy compared to XR-VLM. In general, our method achieves the highest accuracy on most tasks, and the consistent improvements over state-of-the-art baselines underscore the importance of cross-relationship modeling and multi-part feature learning in addressing the challenges of FGVR.

4.3. Ablation Study

To fully explore the reasons for the superior performance of the proposed method and inspire the follow-up research work, we take a comprehensive ablation study. The experiments are conducted on CUB-200-2011 and Stanford-Cars datasets, two standard fine-grained image analysis datasets. The former are natural creatures, usually named by biological experts, whose names reflect some of their own

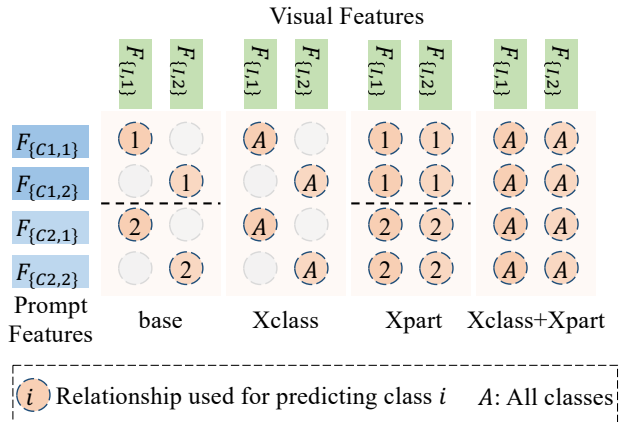


Figure 4. Illustration of different cross relationships for prediction.

attributes (Black footed Albatross, White necked Raven), while the latter are a typical class of artificial creatures, whose names contain fewer categorical attributes (Audi S4 Sedan 2012, BMW M5 Sedan 2010).

4.3.1. Comparison of Different Prediction Strategies.

We propose a cross relationship modeling scheme for prediction, which enables 1-to-many information utilization of prompt and visual features. In this section, we demonstrate its effectiveness for VLM-based FGVR by comparing it with other prediction strategies. The results are presented in Table 2, where MLPs refers to adding an MLP block as the

Visual Encoder	Strategy	Datasets			
		CUB-200-2011		Stanford-Cars	
RN50	PLOT	67.31	Ref.	72.99	Ref.
	MLPs	67.81	$\Delta 0.50$	73.28	$\Delta 0.28$
	PwCS	70.97	$\Delta 3.66$	77.78	$\Delta 4.79$
	CRM	75.68	$\Delta 8.37$	81.75	$\Delta 8.76$
	-base	69.33	$\Delta 2.02$	78.48	$\Delta 5.49$
	-Xpart	66.47	$\nabla 0.84$	77.00	$\Delta 4.01$
	-Xclass	74.61	$\Delta 7.30$	79.87	$\Delta 6.82$
	ViT-B/16	PLOT	77.55	Ref.	84.42
MLPs	76.70	$\nabla 0.85$	81.67	$\nabla 2.75$	
PwCS	77.37	$\nabla 0.18$	84.61	$\Delta 0.19$	
CRM	81.08	$\Delta 3.53$	86.52	$\Delta 2.10$	
-base	76.60	$\nabla 0.95$	84.70	$\Delta 0.28$	
-Xpart	76.42	$\nabla 1.13$	85.53	$\Delta 1.11$	
-Xclass	79.11	$\Delta 1.56$	86.04	$\Delta 1.62$	

Table 2. Performance of different prediction strategies.

classifier for visual features, and **PwCS** denotes calculating the similarity between each pair of textual and visual features, as formulated in Eq. (7). For the proposed CRM, as shown in Fig. 4, we evaluate four variants: the base version, Xclass, Xpart, and the full version (Xclass+Xpart). Details of these methods can be found in supplementary material. PLOT is adopted as the baseline since it also interpolates multiple prompts into VLMs.

We can see that for RN50 visual encoder, PwCS, MLPs, and CRM all achieve better performance than PLOT, and CRM can obtain obvious improvements of 8.37% and 8.76%, respectively. As for the ViT encoder, even PLOT achieves better performance than MLPs and PwCS, our proposed CRM still obtains 3.53% and 2.10% gains than it. The results demonstrate that: (1) learning multiple prompts can significantly boost the performance on CLIP on fine-grained image classification, but how to utilize it has a significant impact on performance; (2) aligning multiple prompts to multiple visual part features can obtain better performance than to multiple visual local features; (3) the proposed cross relationship modeling module can better explore the correlations between visual and textual information than just part-wise similarity calculating.

4.3.2. Different Number of Prompts/Visual Features.

Our proposed XR-VLM processes multiple prompts and visual features for prediction. To assess the impact of varying numbers of prompts and visual features, we conduct experiments and compare our method with PLOT. The results are presented in Fig. 5. As the number of prompt/visual representations increases, our method consistently outperforms PLOT across most of settings, demonstrating superior adaptability and robustness in fine-grained recognition. Specifically, (1) our method usually achieves

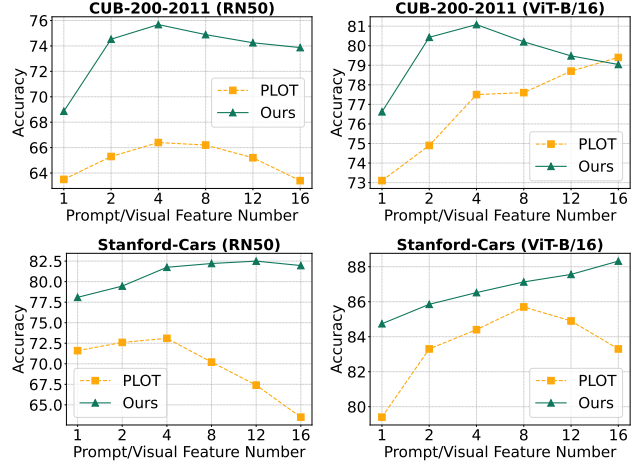


Figure 5. Comparison between PLOT and our method with different number of Prompt/Visual features and image encoders.

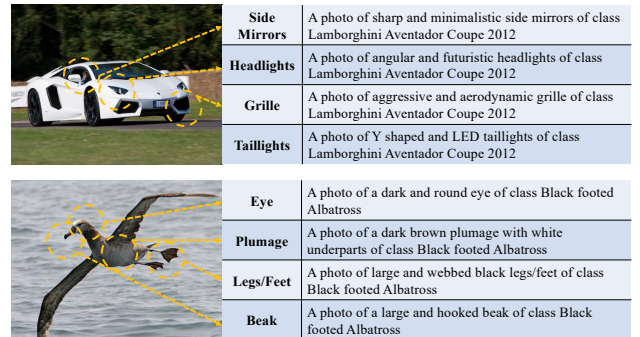


Figure 6. Examples of part descriptions generated by LLM. We let LLM generate 4 key names of each dataset and corresponding part descriptions of each sub-categories.

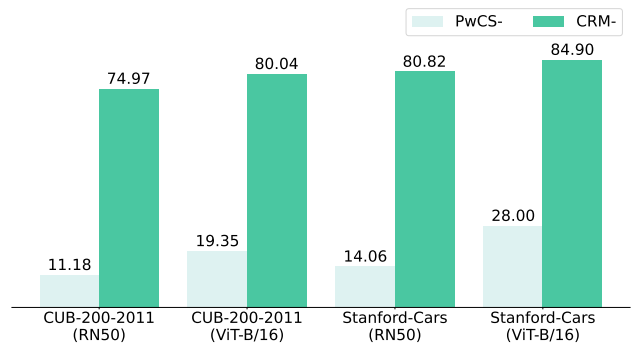


Figure 7. Performance on manual prompts. PwCS- and CRM- denotes modeling relationship between manual prompts and visual features by PwCSa and our CRM modules, respectively.

significantly higher accuracy than PLOT across different dataset-backbone combinations. This indicates that modeling crossing relationship can effectively enhances fine-grained recognition; (2) for the ViT-B/16 backbone, while

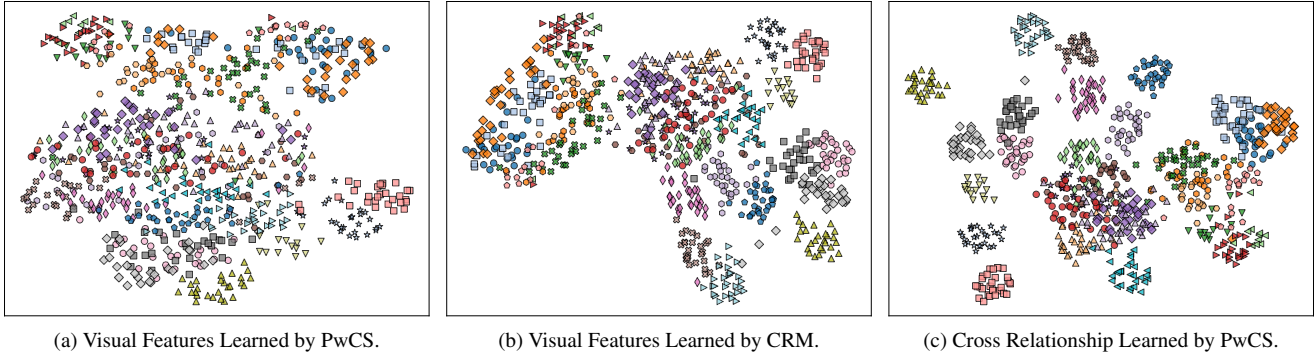


Figure 8. UMAP visualization of learned features. Different shape-color combinations denote different classes. Data are selected from CUB-200-2011 datasets, and the first 30 classes are shown for clarity of presentation. (best view in color)

PLOT exhibits performance degradation as the number of prompts/visual representations increases, our method maintains stable or improving trends. Notably, although a larger number of prompts/visual features generally leads to better performance, an excessive number introduces more learnable parameters, which can slow down the inference speed of the text encoder. To balance performance and efficiency, we set the number to 4 as default.

4.3.3. Compatible with Manual Prompts.

In this work, we propose a novel prediction pattern that takes a further step in leveraging both prompt and visual features for fine-grained recognition. Our method not only integrates these two modalities but also treats their interaction as a discriminative representation. By default, multi-part prompts are learned through back-propagation, ensuring adaptive optimization, while this pattern also supports manually designed prompts for greater flexibility. To achieve this, we utilize a large language model, DeepSeek-V3, to generate a set of part-level descriptions for the CUB-200-2011 and Stanford-Cars datasets as the prompts. Some examples are shown in Fig. 6. By comparing the images with their corresponding descriptions, we observe that some generated descriptions can effectively capture fine-grained class-specific details, but there are some words that struggle to express category-specific features, *e.g.*, ‘aggressive and aerodynamic grille’. The results are shown in Fig. 7. We can find that PwCS is hard to handle these manual prompts but our method can still achieve high performance, just a little lower than using learnable prompts.

4.4. Visualization

Features Visualization. To demonstrate the discriminative power of cross-relationship modeling, we visualize the visual features and cross relationships by UMAP [21] technology in Fig. 8. As shown in the figure, the visual features from the PwCS are difficult to distinguish on the 2D plane, and while some classes from CRM exhibit clustering, the

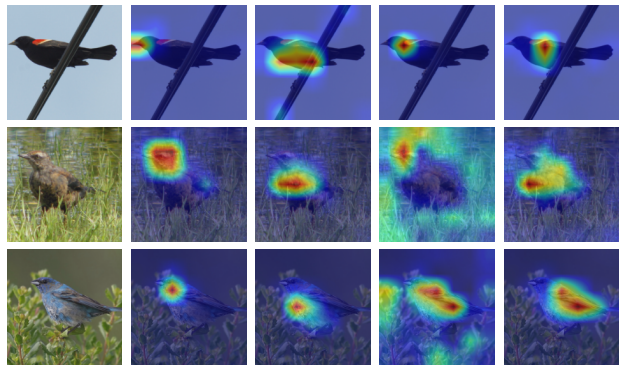


Figure 9. Visualization of learned attentions.

separation is still not pronounced. In contrast, the cross relationship of each class is relatively distinct, highlighting its discriminative capability and explaining the significant performance improvement observed in our experiments.

Attention Visualization. Then, we visualize the generated attention masks in Fig. 9 to provide insights into the characteristics of the visual features. As shown in the figure, for each input image (first column), the generated attention masks effectively cover different parts of the birds. This demonstrates that the unified attention module successfully extracts discriminative multi-part visual features, thereby enhancing the effectiveness of cross-relationship modeling.

5. Conclusion

In this paper, we find that current fine-tuning methods for VLMs like CLIP face challenges to the task of fine-grained visual recognition. We argue that this limitation stems from restricted prompt/feature learning and insufficient utilization of relationships between modalities. To address this, we propose a multi-part prompt learning and utilization method that learns both multiple textual and visual features and deeply leverages their relationships for FGVR. Experimental results demonstrate that our method achieves

state-of-the-art performance across various benchmark fine-grained datasets, outperforming a wide range of existing methods. We should acknowledge that current method does not take the domain generalization into consideration and we think it is not in the scope of this work, and we will focus on how to model adaptive relationship for incremental learning and base-to-novel learning in the future.

References

- [1] Guangyi Chen, Tianpei Gu, Jiwen Lu, Jinan Bao, and Jie Zhou. Person re-identification via attention pyramid. *IEEE TIP*, 30:7663–7676, 2021. 3
- [2] Guangyi Chen, Weiran Yao, Xiangchen Song, Xinyue Li, Yongming Rao, and Kun Zhang. PLOT: prompt learning with optimal transport for vision-language models. In *ICLR*. OpenReview.net, 2023. 3, 5, 6
- [3] Alexey Dosovitskiy, Lucas Beyer, Alexander Kolesnikov, Dirk Weissenborn, Xiaohua Zhai, Thomas Unterthiner, Mostafa Dehghani, Matthias Minderer, Georg Heigold, Sylvain Gelly, Jakob Uszkoreit, and Neil Houlsby. An image is worth 16x16 words: Transformers for image recognition at scale. In *ICLR*. OpenReview.net, 2021. 4
- [4] Yu Du, Fangyun Wei, Ziheng Zhang, Miaoqing Shi, Yue Gao, and Guoqi Li. Learning to prompt for open-vocabulary object detection with vision-language model. In *CVPR*, pages 14064–14073. IEEE, 2022. 1
- [5] Jianlong Fu, Heliang Zheng, and Tao Mei. Look closer to see better: Recurrent attention convolutional neural network for fine-grained image recognition. In *CVPR*, pages 4476–4484, 2017. 3
- [6] Peng Gao, Shijie Geng, Renrui Zhang, Teli Ma, Rongyao Fang, Yongfeng Zhang, Hongsheng Li, and Yu Qiao. Clip-adapter: Better vision-language models with feature adapters. *IJCV*, 132(2):581–595, 2024. 2, 5, 6
- [7] Kaiming He, Xiangyu Zhang, Shaoqing Ren, and Jian Sun. Deep residual learning for image recognition. In *CVPR*, pages 770–778. IEEE Computer Society, 2016. 1, 4
- [8] Grant Van Horn, Steve Branson, Ryan Farrell, Scott Haber, Jessie Barry, Panos Ipeirotis, Pietro Perona, and Serge J. Belongie. Building a bird recognition app and large scale dataset with citizen scientists: The fine print in fine-grained dataset collection. In *CVPR*, pages 595–604, 2015. 5
- [9] Edward J. Hu, Yelong Shen, Phillip Wallis, Zeyuan Allen-Zhu, Yuanzhi Li, Shean Wang, Lu Wang, and Weizhu Chen. Lora: Low-rank adaptation of large language models. In *ICLR*. OpenReview.net. 1
- [10] Jie Hu, Li Shen, Samuel Albanie, Gang Sun, and Enhua Wu. Squeeze-and-excitation networks. *IEEE TPAMI*, 42:2011–2023, 2017. 3
- [11] Tao Hu and Honggang Qi. See better before looking closer: Weakly supervised data augmentation network for fine-grained visual classification. *CoRR*, abs/1901.09891, 2019. 3
- [12] Yunshi Huang, Fereshteh Shakeri, Jose Dolz, Malik Boudiaf, Houda Bahig, and Ismail Ben Ayed. LP++: A surprisingly strong linear probe for few-shot CLIP. In *CVPR*, pages 23773–23782. IEEE, 2024. 3, 5, 6
- [13] Chao Jia, Yinfei Yang, Ye Xia, Yi-Ting Chen, Zarana Parekh, Hieu Pham, Quoc V. Le, Yun-Hsuan Sung, Zhen Li, and Tom Duerig. Scaling up visual and vision-language representation learning with noisy text supervision. In *ICML*, pages 4904–4916. PMLR, 2021. 1
- [14] Muhammad Uzair Khattak, Hanoona Abdul Rasheed, Muhammad Maaz, Salman H. Khan, and Fahad Shahbaz Khan. Maple: Multi-modal prompt learning. In *CVPR*, pages 19113–19122. IEEE, 2023. 2, 5, 6
- [15] Muhammad Uzair Khattak, Syed Talal Wasim, Muzammal Naseer, Salman Khan, Ming-Hsuan Yang, and Fahad Shahbaz Khan. Self-regulating prompts: Foundational model adaptation without forgetting. In *ICCV*, pages 15144–15154. IEEE, 2023. 2, 5, 6
- [16] Aditya Khosla, Nityananda Jayadevaprakash, Bangpeng Yao, and Li Fei-Fei. Novel dataset for fine-grained image categorization. In *CVPRW*, 2011. 5
- [17] Jonathan Krause, Michael Stark, Jia Deng, and Li Fei-Fei. 3d object representations for fine-grained categorization. In *ICCVW*, pages 554–561, 2013. 5
- [18] Zheng Li, Xiang Li, Xinyi Fu, Xin Zhang, Weiqiang Wang, Shuo Chen, and Jian Yang. Promptkd: Unsupervised prompt distillation for vision-language models. In *CVPR*, pages 26607–26616. IEEE, 2024. 2, 5
- [19] Tsung-Yu Lin, Aruni RoyChowdhury, and Subhransu Maji. Bilinear CNN models for fine-grained visual recognition. In *ICCV*, pages 1449–1457, 2015. 3
- [20] S. Maji, J. Kannala, E. Rahtu, M. Blaschko, and A. Vedaldi. Fine-grained visual classification of aircraft. Technical report, 2013. 5
- [21] Leland McInnes and John Healy. UMAP: uniform manifold approximation and projection for dimension reduction. *CoRR*, abs/1802.03426, 2018. 8
- [22] Alec Radford, Jong Wook Kim, Chris Hallacy, Aditya Ramesh, Gabriel Goh, Sandhini Agarwal, Girish Sastry, Amanda Askell, Pamela Mishkin, Jack Clark, Gretchen Krueger, and Ilya Sutskever. Learning transferable visual models from natural language supervision. In *ICML*, pages 8748–8763. PMLR, 2021. 1, 5, 6
- [23] Yongming Rao, Guangyi Chen, Jiwen Lu, and Jie Zhou. Counterfactual attention learning for fine-grained visual categorization and re-identification. In *ICCV*, pages 1005–1014, 2021. 3
- [24] Shaoqing Ren, Kaiming He, Ross B. Girshick, and Jian Sun. Faster R-CNN: towards real-time object detection with region proposal networks. In *NIPS*, pages 91–99, 2015. 3
- [25] Karen Simonyan and Andrew Zisserman. Very deep convolutional networks for large-scale image recognition. In *ICLR*, 2015. 1
- [26] Chuanming Wang, Huiyuan Fu, and Huadong Ma. Learning mutually exclusive part representations for fine-grained image classification. *IEEE TMM*, 26:3113–3124, 2024. 3, 4
- [27] Yaming Wang, Vlad I. Morariu, and Larry S. Davis. Learning a discriminative filter bank within a CNN for fine-grained recognition. In *CVPR*, pages 4148–4157, 2018. 3
- [28] P. Welinder, S. Branson, T. Mita, C. Wah, F. Schroff, S. Belongie, and P. Perona. Caltech-UCSD Birds 200. Technical

Report CNS-TR-2010-001, California Institute of Technology, 2010. 5

- [29] Hu Xu, Gargi Ghosh, Po-Yao Huang, Dmytro Okhonko, Armen Aghajanyan, Florian Metze, Luke Zettlemoyer, and Christoph Feichtenhofer. Videoclip: Contrastive pre-training for zero-shot video-text understanding. In *EMNLP*, pages 6787–6800. Association for Computational Linguistics, 1
- [30] Lian Xu, Wanli Ouyang, Mohammed Bennamoun, Farid Boussaïd, and Dan Xu. Multi-class token transformer for weakly supervised semantic segmentation. In *CVPR*, pages 4300–4309. IEEE, 2022. 3
- [31] Lingxiao Yang, Ru-Yuan Zhang, Yanchen Wang, and Xiaohua Xie. MMA: multi-modal adapter for vision-language models. In *CVPR*, pages 23826–23837. IEEE, 2024. 1, 2, 5, 6
- [32] Xuhui Yang, Yaowei Wang, Ke Chen, Yong Xu, and Yonghong Tian. Fine-grained object classification via self-supervised pose alignment. In *CVPR*, pages 7389–7398, 2022. 3
- [33] Lewei Yao, Runhui Huang, Lu Hou, Guansong Lu, Minzhe Niu, Hang Xu, Xiaodan Liang, Zhenguo Li, Xin Jiang, and Chunjing Xu. FILIP: fine-grained interactive language-image pre-training. In *ICLR*. OpenReview.net, 2022. 1
- [34] Xiaohua Zhai, Xiao Wang, Basil Mustafa, Andreas Steiner, Daniel Keysers, Alexander Kolesnikov, and Lucas Beyer. Lit: Zero-shot transfer with locked-image text tuning. In *CVPR*, pages 18102–18112. IEEE, 2022. 1
- [35] Ning Zhang, Jeff Donahue, Ross B. Girshick, and Trevor Darrell. Part-based r-cnns for fine-grained category detection. In *ECCV*, pages 834–849, 2014. 2, 3
- [36] Renrui Zhang, Wei Zhang, Rongyao Fang, Peng Gao, Kunchang Li, Jifeng Dai, Yu Qiao, and Hongsheng Li. Tip-adapter: Training-free adaption of CLIP for few-shot classification. In *ECCV*, pages 493–510. Springer, 2022. 2, 5, 6
- [37] Heliang Zheng, Jianlong Fu, Zheng-Jun Zha, and Jiebo Luo. Looking for the devil in the details: Learning trilinear attention sampling network for fine-grained image recognition. In *CVPR*, pages 5012–5021, 2019. 3
- [38] Kaiyang Zhou, Jingkang Yang, Chen Change Loy, and Ziwei Liu. Conditional prompt learning for vision-language models. In *CVPR*, pages 16795–16804. IEEE, 2022. 2, 5
- [39] Kaiyang Zhou, Jingkang Yang, Chen Change Loy, and Ziwei Liu. Learning to prompt for vision-language models. *IJCV*, 130(9):2337–2348, 2022. 1, 2, 3, 4, 5, 6
- [40] Beier Zhu, Yulei Niu, Yucheng Han, Yue Wu, and Hanwang Zhang. Prompt-aligned gradient for prompt tuning. In *ICCV*, pages 15613–15623. IEEE, 2023. 5, 6
- [41] Muzhi Zhu, Hengtao Li, Hao Chen, Chengxiang Fan, Weian Mao, Chenchen Jing, Yifan Liu, and Chunhua Shen. Seg-prompt: Boosting open-world segmentation via category-level prompt learning. In *ICCV*, pages 999–1008. IEEE, 2023. 1

XR-VLM: Cross-Relationship Modeling with Multi-part Prompts and Visual Features for Fine-Grained Recognition

Supplementary Material

6. Similarity between Fine-grained Classes

Fine-grained visual recognition focuses on distinguishing sub-categories within a broader superclass, where the similarity among these sub-categories is significantly higher compared to coarse-grained classes, often leading to confusion in predictions. The high similarity between class names also poses a challenge for VLMs, which rely on class names as the basis for classification, making it difficult to obtain discriminative features. In this section, we demonstrate this through a simple experiment and visualization. We evaluate the Stanford-Cars and CIFAR-100 datasets, using the ViT-B/16 text encoder from CLIP. All class names from both datasets are encoded by the text encoder, and we apply UMAP to visualize their embeddings.

As shown in Fig. 10 (in next page), from the visualization, we observe that the Class Name Embeddings (CNEs) in CIFAR-100 are more evenly distributed, whereas those in Stanford-Cars are closer to each other in the embedding space. This indicates that distinguishing fine-grained categories based solely on category names is more challenging for Stanford-Cars, as the semantic differences between class names are less pronounced. In the first column of Fig. 10, we highlight some class names that are close to each other, showing that their names are highly similar, differing only in model types. Consequently, a simple alignment-based prediction method would struggle to learn discriminative features for fine-grained recognition in such scenarios.

To further quantitatively analyze the similarity of CNEs across different datasets, we calculate the distance between each CNE and its nearest neighbor and plot the corresponding histogram (third column of Fig. 10). The histogram for CIFAR-100 is relatively flat, with most distances being less than 7. In contrast, for Stanford-Cars, most minimum distances are greater than 6, indicating that the class names are much more similar.

7. Details of Unified Attention Module

Since there are two architectures (ResNet and Vision Transformer) of visual encoder in CLIP, and their outputs are different in shapes. In Section 3.4, we introduce an unified attention module to extract multi-part visual features that can fit with these two types of architectures. Thus, in this part, we detail how it works for different architectures.

For ResNet in CLIP, it consists of one input term block (Conv-BN-ReLU-Maxpool), four residual layers, and one attention pooling layer. The attention pooling layer is im-

plemented by a multihead attention module, and it can be formulated as:

$$\mathbf{F} = \text{softmax} \left(\frac{\bar{\mathbf{X}} \mathbf{W}_q (\bar{\mathbf{X}} \mathbf{W}_k)^\top}{\sqrt{d_k}} \right) (\bar{\mathbf{X}} \cdot \mathbf{W}_v) \mathbf{W}_c, \quad (10)$$
$$\bar{\mathbf{X}} = [\text{AVG}_{2D}(\mathbf{X}), \epsilon(\mathbf{X}, (HW \times C))] + \mathbf{P}.$$

In Eq. (10), $\mathbf{X} \in \mathbb{R}^{C \times H \times W}$ is the output of residual layers and input of attention pooling layer, AVG_{2D} denotes the average pooling layer for the spatial dimension, ϵ is the reshape operation that re-arrange the shape of \mathbf{X} to $HW \times C$, and $\mathbf{P} \in \mathbb{R}^{(1+HW) \times C}$ is the position embeddings. Then the self-attention operation is performed on $\bar{\mathbf{X}}$ and outputs $\mathbf{F} \in \mathbb{R}^{(1+HW) \times C}$. In the original CLIP, the first feature in \mathbf{F} is selected as the output of the attention pooling layer, but it losses too many spatial information for part feature learning. Thus, keeping the parameters fixed, we simplify the visual feature learning process as:

$$\mathbf{F} = \epsilon((\bar{\mathbf{X}} \mathbf{W}_v) \mathbf{W}_c, HW \times C) \in \mathbb{R}^{HW \times C}. \quad (11)$$

Then, \mathbf{F} is sent to our proposed unified attention module for multi-part visual feature learning.

As for Vision Transformer, it outputs \mathbf{F} with shape $N \times C$ as the output of the image encoder, we directly use it as the input of our unified attention module for multi-part visual feature learning.

8. Details of Prediction Strategy.

In Section 4.3.1 of the main text, we introduce various prediction strategies to demonstrate that our proposed CRM can achieve optimal performance. In addition to the **PwCS** introduced in Eq. (7), we will describe the remaining prediction strategies in this part.

MLPs. To maintain consistency with the symbols used in the main text, we denote the multi-part visual features as $\mathbf{V} \in \mathbb{R}^{S \times E}$, where S represents the number of parts and E is the feature dimension. We employ N MLPs, denoted as $\{f_1, \dots, f_N\}$, as classifiers, and their outputs are averaged to produce the final prediction:

$$\hat{\mathbf{y}} = \frac{1}{N} \sum_i^S f_i(\mathbf{V}_i). \quad (12)$$

Then, the loss is computed using the cross-entropy loss function between the predicted output $\hat{\mathbf{y}}$ and the ground-truth labels \mathbf{y} , optimizing the parameters in prompts, the Unified Attention module, and the MLPs. Although no

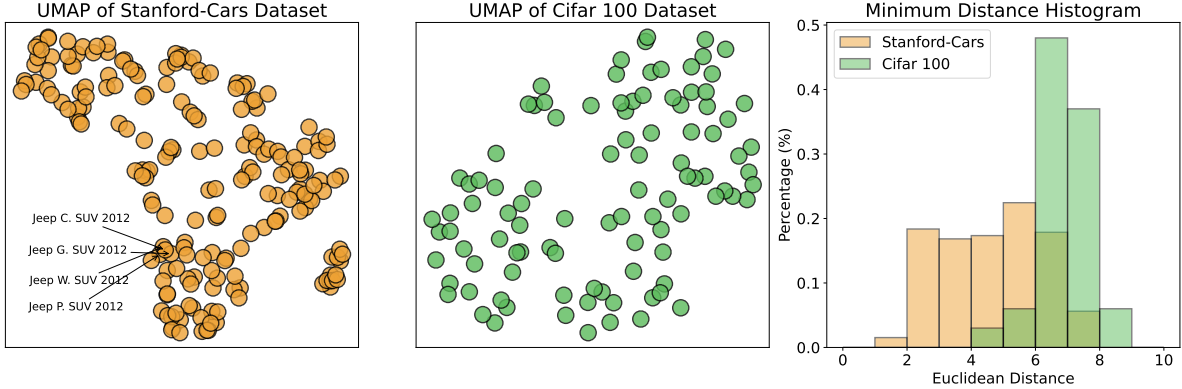


Figure 10. UMAP of class name embeddings and minimum distance histogram.

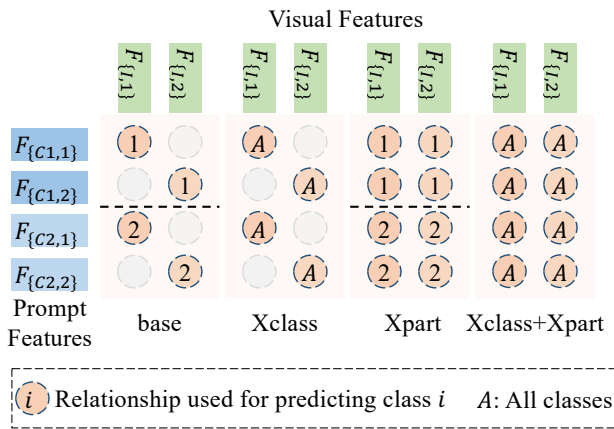


Figure 11. Illustration of different cross relationships for prediction.

language information is used in this prediction, the results are still comparable to those of CoOp on the CUB-200-2011 and Stanford-Cars datasets. This indicates that learning multi-part visual features is beneficial for VLM-based FGVR. However, its performance remains significantly lower than that of the CRM strategy, underscoring the importance of leveraging both visual and language information in VLMs.

CRM-base. Let the learned cross relationship from Eq. (8) be denoted as $\mathbf{R} \in \mathbb{R}^{S \times W}$, where W is the number of classes in the current dataset. We first reshape \mathbf{R} to the shape of $W \times S \times S$. Then, we pass it through an MLP layer f (output dimension is 1) to obtain the final prediction, formulated as:

$$\hat{\mathbf{y}} = \epsilon([f(\epsilon(\mathbf{R}_1 \mathbf{I}_S)), \dots, f(\epsilon(\mathbf{R}_W \mathbf{I}_S))]) \in \mathbb{R}^W, \quad (13)$$

where ϵ denotes the flatten operation, \mathbf{I}^S is the identity matrix, and $[\dots]$ represents the concatenation operation.

For clarity, we include Fig. 4 of the main text here as Fig. 11. By using the identity matrix, the cross-part relationships are masked, and the relationship with number 1 is

used to predict the probability of class 1, and so on.

CRM-Xclass. Same with CRM-base, we employ \mathbf{R} to denote the learned cross relationships, and we still adopt a MLP to output the prediction, but its output dimension is W . It can be formulated as:

$$\hat{\mathbf{y}} = f([\mathbf{R}_1 \mathbf{I}_S, \dots, \mathbf{R}_W \mathbf{I}_S]) \in \mathbb{R}^W. \quad (14)$$

CRM-Xpart. Still denote \mathbf{R} the cross relationships, the prediction of CRM-Xclass can be formulated as:

$$\hat{\mathbf{y}} = \epsilon([f(\epsilon(\mathbf{R}_1)), \dots, f(\epsilon(\mathbf{R}_W))]) \in \mathbb{R}^W, \quad (15)$$

where f is a MLP, and its output dimension is 1.

9. Manual Prompts

In Section 4.3.3, we introduce manual prompts to demonstrate the robustness of our proposed Cross-Relationship Modeling to different prompts. We detail the process of generating these prompts and provide additional examples in this section.

Table 3 outlines the instructions used to generate the manual prompts. We first instruct a LLM, specifically DeepSeek-V3 in our experiments, to output four key part names that can be used to distinguish different sub-categories. For example, it generates ‘side mirrors’, ‘headlights’, ‘grille’, and ‘taillights’ for cars, and ‘eye’, ‘beak’, ‘legs/feet’, and ‘plumage’ for birds. Next, we provide the LLM with a class name and ask it to generate descriptions of that class based on the previously identified parts.

In Fig. 12, we present additional manual prompts. It is evident that the quality of the generated descriptions is inconsistent, with some descriptions being overly vague and failing to accurately capture the characteristics of the target class. We speculate that this issue may arise from two factors: (1) LLM may require more fine-tuned instructions to produce higher-quality part descriptions, and (2) describing the characteristics of fine-grained sub-categories in explicit language may be inherently challenging, even for advanced language models.

Roles	Content
User	I am doing fine-grained image classification, can you provide the names of 4 key parts to distinguish different cars? Just give me the answer.
LLM	[headlights, grille, side mirrors, taillights]
User	The user is performing fine-grained image classification and will provide a car class name along with the names of a set of key parts. You need to do the following: Based on the provided parts, describe their appearance for the given car class, avoiding abstract words.
User	Lamborghini Aventador Coupe 2012, [headlights, grille, side mirrors, taillights]
LLM	headlights: a photo of angular and futuristic headlights of class Lamborghini Aventador Coupe 2012, grille: a photo of aggressive and aerodynamic grille of class Lamborghini Aventador Coupe 2012, side mirrors: a photo of sharp and minimalistic side mirrors of class Lamborghini Aventador Coupe 2012, taillights: a photo of Y shaped and LED taillights of class Lamborghini Aventador Coupe 2012.

Table 3. Instructions for LLM to generate part-level descriptions.


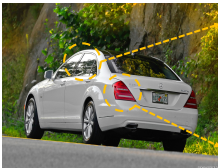
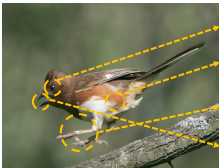



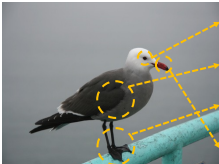
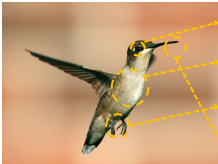
	Side Mirrors	A photo of wide, heated side mirrors of class Honda Odyssey Minivan 2012		Side Mirrors	A photo of auto-dimming, power-folding side mirrors of class Mercedes-Benz S-Class Sedan 2012
	Headlights	A photo of practical, halogen headlights of class Honda Odyssey Minivan 2012		Headlights	A photo of advanced, intelligent headlights of class Mercedes-Benz S-Class Sedan 2012
	Grille	A photo of a family-friendly, chrome grille of class Honda Odyssey Minivan 2012		Grille	A photo of a prominent, chrome grille of class Mercedes-Benz S-Class Sedan 2012
	Taillights	A photo of clear, functional taillights of class Honda Odyssey Minivan 2012		Taillights	A photo of sophisticated, LED taillights of class Mercedes-Benz S-Class Sedan 2012
	Eye	A photo of a dark and round eye of class Eastern Towhee		Eye	A photo of a dark and intelligent eye of class Fish Crow
	Plumage	A photo of a black upper body with white underparts and reddish sides of class Eastern Towhee		Plumage	A photo of glossy black plumage of class Fish Crow
	Legs/Feet	A photo of strong and brown legs/feet of class Eastern Towhee		Legs/Feet	A photo of robust and clawed legs/feet of class Fish Crow
	Beak	A photo of a short and stout beak of class Eastern Towhee		Beak	A photo of a strong and slightly curved beak of class Fish Crow
	Side Mirrors	A photo of practical and durable side mirrors of class Jeep Patriot SUV 2012		Side Mirrors	A photo of rounded side mirrors with turn signals of class Hyundai Veracruz SUV 2012
	Headlights	A photo of versatile and reliable headlights of class Jeep Patriot SUV 2012		Headlights	A photo of bold, multi-lens headlights of class Hyundai Veracruz SUV 2012
	Grille	A photo of a classic and rugged grille of class Jeep Patriot SUV 2012		Grille	A photo of a chrome-trimmed grille of class Hyundai Veracruz SUV 2012
	Taillights	A photo of sturdy and functional taillights of class Jeep Patriot SUV 2012		Taillights	A photo of dual-element taillights of class Hyundai Veracruz SUV 2012
	Eye	A photo of a dark eye of class Heermann Gull		Eye	A photo of a small black Eye of class Ruby throated Hummingbird
	Plumage	A photo of a slate-gray plumage with a white head of class Heermann Gull		Plumage	A photo of an iridescent green Plumage of class Ruby throated Hummingbird
	Legs/Feet	A photo of red legs and feet of class Heermann Gull		Legs/Feet	A photo of tiny delicate Legs/Feet of class Ruby throated Hummingbird
	Beak	A photo of a red beak with a black tip of class Heermann Gull		Beak	A photo of a long slender Beak of class Ruby throated Hummingbird

Figure 12. Additional examples of manual prompts for CUB-200-2011 and Stanford-Cars datasets.

10. Computational Overhead

We acknowledge that multi-part prompt/feature learning introduces additional parameters, which may increase inference time. Here, we provide a detailed analysis. When the number of prompts/visual features is set to 4 and the image encoder is RN50, the trainable parameters for the CUB-200-2011 dataset total 11.1M, distributed as follows: prompts account for 6.6M parameters, the Unified Attention module contains 14.3K parameters, and the classifier comprises 4.5M parameters. Compared to the original CLIP, which has 76.7M parameters, the trainable parameters in

our method are relatively small, representing only 12.6% of total parameters. For ViT-B/16, this percentage decreases to 7.7%.

Additionally, we evaluate the inference time of our method against CoOp. The results show that CoOp and our method takes 13.4 ms and 15.3 ms for RN50, and 21.95 ms and 41.8 ms for ViT-B/16, respectively. In future work, we will explore ways to optimize inference speed and reduce the number of learnable parameters by matrix decomposition, q-former or other strategies.